# Compensation of Gravitational Perturbations for Precise Formation Flying in Low Earth Orbit

Takahiro Ito [(1)]

[(1)]*Institute of Space and Astronautical Science, Japan Aerospace Exploration Agency*
*Sagamihara, Japan*
*Email:ito.takahiro@jaxa.jp*

***Abstract* – Precise satellite formation flying is a promising technology to enable unprecedented astronomical observations in space. To pave pathways to comprehensive astronomical missions, preliminary missions involving small satellites in low Earth orbit (LEO) have been proposed. However, there exist various perturbation sources in LEO, and their compensation is essential to keep the rigid and precise formation. This study proposes the feedforward control method to compensate gravitational perturbations, which can be predicted accurately from spacecraft's absolute position. The numerical analysis shows that the feedforward control could reduce the load of the feedback controller significantly, which potentially makes precise formation flying in LEO much easier.**

## I. INTRODUCTION

Spacecraft formation flying enables the construction of large virtual structures in space. Precise formation flying missions have been proposed and ongoing in the world. For example, PROBA-3 [1] will demonstrate several formation activities including coarse-to-fine control, autonomy, safety management, and solar coronagraph observation in a highly elliptical orbit (HEO). PROBA-3 can resize its baseline length between 25 m and 250 m while maintaining sub-milli-meter- and arc-second-order relative displacement and pointing accuracy.

Some formation-flying astronomical missions using interferometric techniques require further control accuracy of less than 1 $\mu$m between science instruments. To provide a pathway towards future comprehensive missions, smaller-class space missions have been proposed by using a near-circular low Earth orbit (LEO). One representative is a linear astronomical interferometer (cf., [2, 3]), which comprises one beam combiner spacecraft and two collector spacecraft. Their formation size is kept about tens to hundreds of meters, and it typically requires the $\mu$m-level control accuracy of the optical path difference from stellar light. To attain this control accuracy between the science instruments, the relaxed but still challenging (e.g., mm-level) control accuracy between the satellites would be necessary by rigid and continuous formation control.

It was sufficient for the typical formation flying missions being operational in LEO to compensate long-period and secular perturbations, and control the mean relative orbital elements. However, formation flying interferometry typically requires the rigid and continuous formation keeping for intended observations. Therefore, it is essential for formation flying interferometry in LEO to mitigate short-period perturbations, and control osculating relative motion precisely. In addition, different from precise formation flying at apogee in HEO, that in LEO involves various perturbation sources. These perturbations include, for example, the Earth $J_2$ gravitational potential, long-period drift of eccentricity vector, third-body gravity, nonlinear terms of linearized relative motion, atmospheric drag, and solar radiation pressure. Atmospheric drag and solar radiation pressure have environmental and systematic uncertainties. On the other hand, the other perturbations are caused by Earth or third-body gravity, so that their effects tend to be deterministic. Thus, they are potentially compensated in a feedforward manner.

This study proposes a feedforward control method to attain precise formation flying in a near-circular LEO. The proposed method can compensate the relative short-period perturbations derived from gravity in addition to the long-period and secular ones, which could contribute to attaining the precise formation flying in LEO much easier. The remainder of the paper is organized as follows. Section II reviews the perturbed orbital motion in Earth orbit. Section III proposes the feedforward control law to compensate gravitational perturbations. Section IV shows the validity of the proposed method by closed-loop numerical simulations. Section V provides the conclusions and future work.

## II. RELATIVE ORBITAL MOTION

For unperturbed orbital motion, the linearized relative dynamics in a circular orbit, known as Clohessy-Wiltshire (CW) equation [4], is

$$\ddot{\boldsymbol{r}} = A_{u1}\boldsymbol{r} + A_{u2}\dot{\boldsymbol{r}} + \boldsymbol{u}_d \tag{1}$$

where $\boldsymbol{r}$ is the position vector of the deputy with respect to the chief in the local-vertical local-horizontal (LVLH) frame, $\boldsymbol{u}_d$ is the control acceleration of the deputy in the LVLH frame, and $A_{u1}$and $A_{u2}$ are defined as

$$A_{u1} = \begin{bmatrix} 3n^2 & 0 & 0 \\ 0 & 0 & 0 \\ 0 & 0 & -n^2 \end{bmatrix}, A_{u2} = \begin{bmatrix} 0 & 2n & 0 \\ -2n & 0 & 0 \\ 0 & 0 & 0 \end{bmatrix} \tag{2}$$

where $n$ is the mean motion of the chief. By applying the initial condition to avoid the along-track drift, the closed-form solution $\boldsymbol{r}_r$ is

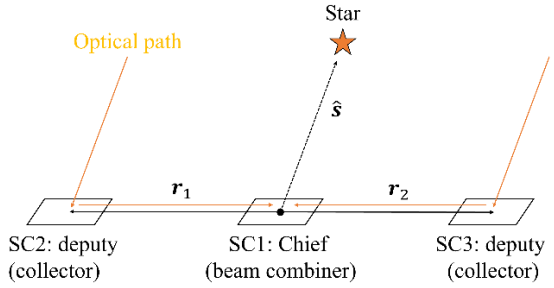


Fig. 1: Schematic of a formation-flying linear astronomical interferometer.

$$\boldsymbol{r}_r = \begin{bmatrix} \rho_x \sin(\theta + \alpha_x) \\ \rho_y + 2\rho_x \cos(\theta + \alpha_x) \\ \rho_z \sin(\theta + \alpha_z) \end{bmatrix} \tag{3}$$

where $\rho_x$, $\rho_y$, $\rho_z$, $\alpha_x$, $\alpha_z$ are the design parameters and $\theta$ is the argument of latitude. This study assumes a linear astronomical interferometer as the benchmark of formation-flying interferometry. Figure 1 shows the schematic of a formation-flying linear astronomical interferometer. The essential requirement on the interferometric observation is to maintain the optical path difference (OPD; $\Lambda$) being sufficiently small [2]. By using the symbols in Fig. 1, this requirement is expressed as

$$\Lambda = (\|\boldsymbol{r}_1\| - \|\boldsymbol{r}_2\| - \hat{\boldsymbol{s}} \cdot \boldsymbol{r}_1 + \hat{\boldsymbol{s}} \cdot \boldsymbol{r}_2) \approx 0 \tag{4}$$

The reference is set for $\hat{\boldsymbol{s}}$ to be perpendicular to $\boldsymbol{r}_1$ and $\boldsymbol{r}_2$, and $\|\boldsymbol{r}_1\| = \|\boldsymbol{r}_2\|$. The linear formation under orthogonal pointing to the star can be configured by setting the design parameters in (3) as follows: one beam combiner spacecraft at the origin and the two collector spacecraft at $\rho_x = 0$, $\rho_y = \pm L$, $\rho_z = \rho_y \tan p \sin(\theta + q)$ [2]. The angles $p$ and $q$ are defined as

$$\begin{cases} \cos p & = \sin \Delta\Omega_\alpha \sin I \cos \delta + \cos I \sin \delta \\ \sin p \sin q & = \sin \Delta\Omega_\alpha \cos I \cos \delta - \sin I \sin \delta \\ \sin p \cos q & = \cos \Delta\Omega_\alpha \cos \delta \end{cases} \tag{5}$$

where $\Delta\Omega_\alpha = (\Omega - \alpha)$, $\Omega$ is the right ascension of the ascending node of the chief, $I$ is the inclination, $\alpha$ and $\delta$ are the right ascension and declination of the target observation direction, respectively. Figure 1 shows the linear formation in Earth orbit to observe the target star.

Next, the perturbed relative motion is [5]

$$\begin{aligned} \ddot{\boldsymbol{r}} = &-2\boldsymbol{\omega} \times \dot{\boldsymbol{r}} - \boldsymbol{\omega} \times (\boldsymbol{\omega} \times \boldsymbol{r}) - \dot{\boldsymbol{\omega}} \times \boldsymbol{r} \\ &+ \boldsymbol{f}_{g2B} + \boldsymbol{f}_p + \boldsymbol{u}_d - \boldsymbol{u}_c \end{aligned} \tag{6}$$

where $\boldsymbol{f}_{g2B}$ is the linearized gravity gradient acceleration owing to the two-body gravitational field, $\boldsymbol{f}_p$ is the relative physical perturbing acceleration, $\boldsymbol{u}_c$ is the absolute control acceleration applied to the chief, and $\boldsymbol{\omega}$ is the orbital angular velocity vector. By defining the positional deviation as $\boldsymbol{\varepsilon} = (\boldsymbol{r} - \boldsymbol{r}_r)$, (6) becomes

$$\ddot{\boldsymbol{\varepsilon}} = A_{t1}\boldsymbol{\varepsilon} + A_{t2}\dot{\boldsymbol{\varepsilon}} + \boldsymbol{f}_p + \boldsymbol{f}_o + \boldsymbol{f}_f + \boldsymbol{u}_d - \boldsymbol{u}_c \tag{7}$$

where $\boldsymbol{f}_o$ is the relative fictitious acceleration owing to the perturbed motion of the chief, $\boldsymbol{f}_f$ is the relative fictitious acceleration owing to the perturbed motion of the reference formation, and $A_{t1}$ and $A_{t2}$ are the matrix in which $n$ in (2) is replaced by $n \to \omega_t$, where $\omega_t$ is the target angular velocity. The form of $\boldsymbol{f}_p$ is determined by each perturbation source, which will be given in [6]. The exact forms of $\boldsymbol{f}_o$ and $\boldsymbol{f}_f$ are [6]

$$\boldsymbol{f}_o = (A_{p1} - A_{t1})\boldsymbol{r} + (A_{p2} - A_{t2})\dot{\boldsymbol{r}} \tag{8}$$

$$\boldsymbol{f}_f = A_{t1}\boldsymbol{r}_r + A_{t2}\dot{\boldsymbol{r}}_r - \ddot{\boldsymbol{r}}_r \tag{9}$$

where

$$A_{p1} = \begin{bmatrix} \omega_z^2 + 2(\mu/R^3) & \dot{\omega}_z & -\omega_x\omega_z \\ -\dot{\omega}_z & \omega_x^2 + \omega_z^2 - (\mu/R^3) & \dot{\omega}_x \\ -\omega_x\omega_z & -\dot{\omega}_x & \omega_x^2 - (\mu/R^3) \end{bmatrix} \tag{10}$$

$$A_{p2} = \begin{bmatrix} 0 & 2\omega_z & 0 \\ -2\omega_z & 0 & 2\omega_x \\ 0 & -2\omega_x & 0 \end{bmatrix} \tag{11}$$

and

$$\begin{cases} \omega_x = \dot{\Omega} \sin I \sin\theta + \dot{I} \cos\theta \\ \omega_z = \dot{\Omega} \cos I + \dot{\theta} \end{cases} \tag{12}$$

In general, the absolute perturbations $\boldsymbol{F}_c$ applied to the chief tend to be larger than the relative ones, so that compensating the absolute perturbations by control is an inefficient way. When the absolute perturbations $\boldsymbol{F}_c$ are not compensated (such that $\boldsymbol{u}_c = \boldsymbol{0}$), the three types of relative perturbations ($\boldsymbol{f}_p, \boldsymbol{f}_o, \boldsymbol{f}_f$) have to be compensated by the control acceleration $\boldsymbol{u}_d$ to keep the position and velocity on the reference formation in (3).

## III. Disturbance Compensation

Figure 2 shows the state feedback control diagram to track the reference formation. The feedback control acceleration is expressed as

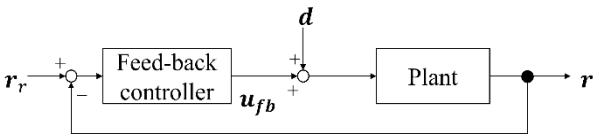


Fig. 2: State feedback control diagram.

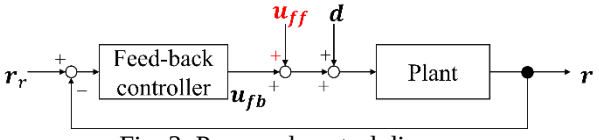


Fig. 3: Proposed control diagram.

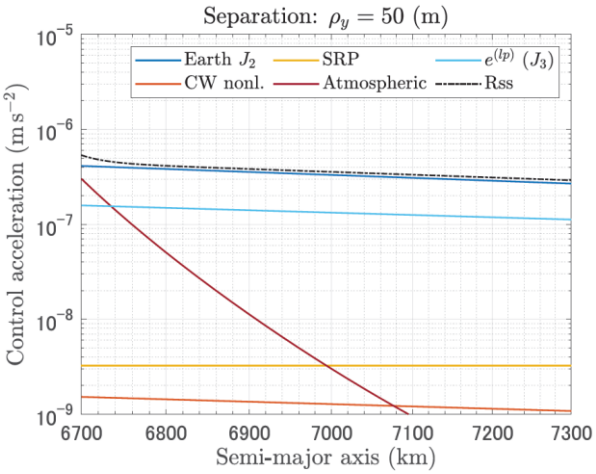


Figure 4: Relative perturbing acceleration in LEO. The calculation condition corresponds to those in Table 2.

$$\boldsymbol{u}_{fb} = -\boldsymbol{K}\boldsymbol{x} \tag{13}$$

where $\boldsymbol{K}$ is the constant gain matrix and $\boldsymbol{x}$ is the state error vector ($\boldsymbol{x} = \begin{bmatrix}\boldsymbol{\varepsilon}^T & \dot{\boldsymbol{\varepsilon}}^T\end{bmatrix}^T$). If the disturbance vector ($\boldsymbol{d}$) in Fig. 2 is non-zero, the control deviation does not reach zero. One possible approach to reduce the deviation is to increase the feedback gain, but the large gain might increase the instability of the control. Another idea is to compensate a large part of $\boldsymbol{d}$ via feedforward control. Figure 3 shows the proposed control diagram. If the feedforward control ($\boldsymbol{u}_{ff}$) can predict the imposed disturbance accurately, $\boldsymbol{u}_{ff}$ gets close to $\boldsymbol{u}_{ff} \to -\boldsymbol{d}$. By combining the feedforward and feedback controls, the control deviation potentially reaches close to zero much easier. The feasibility of this control strategy hinges on whether the disturbance can be known accurately.

The previous study [6] identifies the various perturbation sources existing in Earth orbits for precise formation flying: CW nonlinearity (the non-linear terms which are neglected in the linearization process to attain (1)), Earth $J_2$ gravity, small eccentricity (caused by long-period perturbation via Earth $J_2/J_3$ gravity), lunisolar gravity, atmospheric drag, and solar radiation pressure. Figure 4 shows an example of mean relative perturbing accelerations per revolution in LEO. In Fig. 4, the major gravitational perturbations in LEO are Earth $J_2$ gravity, small eccentricity, and CW nonlinearity. These gravitational perturbations tend to be deterministic. The other gravitational perturbations such as lunisolar gravity and Earth gravity potential higher than $J_3$ term are less than $10^{-9}$ m/s$^2$. On the other hand, the atmospheric drag and solar radiation pressure have environmental or systematic uncertainty, so that it is more challenging to predict these non-gravitational perturbations. However, their magnitudes tend to be smaller than those of the major gravitational perturbations; therefore, they may be potentially neglected or mitigated by the simple gain tuning of the feedback controller.

Table 1: Proposed control strategy to compensate the various perturbations in LEO.

| Perturbations | $\boldsymbol{f}_p$ | $\boldsymbol{f}_o$ | $\boldsymbol{f}_f$ |
|---|---|---|---|
| CW nonlinearity | FF | N/A | N/A |
| Earth $J_2$ gravity | FF | FF | FF |
| Earth $J_n$ gravity ($n \geq 3$) | FB | FB | FB |
| Small eccentricity (by Earth $J_2/J_3$ gravity) | N/A | FF | FF |
| Lunisolar gravity | FB | FB | FB |
| Atmospheric drag | FB | FB | FB |
| Solar radiation pressure | FB | FB | FB |

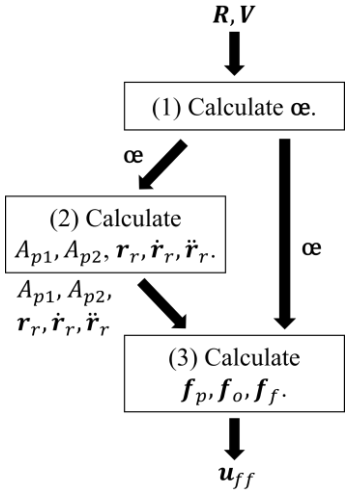


Fig. 5: Flow chart to calculate the feedforward control acceleration.

Table 1 shows the proposed control strategy to compensate various perturbations in LEO. Note that "FF" in Table 1 indicates the disturbances compensated by feedforward control, "FB" indicates those by feedback control, and "N/A" indicates that there is no corresponding disturbance. Figure 5 shows the flow chart to calculate the feedforward control acceleration ($\boldsymbol{u}_{ff}$). The detailed calculation steps are summarized as follows.

1. Calculate the osculating orbital elements: $\text{œ} = [a \quad e_x \quad e_y \quad I \quad \Omega \quad \theta]$ from the present position and velocity ($\boldsymbol{R}$, $\boldsymbol{V}$) of the chief.
2. Calculate $A_{p1}, A_{p2}$ in (10)-(11) and $\boldsymbol{r}_r$, $\dot{\boldsymbol{r}}_r$, $\ddot{\boldsymbol{r}}_r$ in (3) from the analytical models by the input œ.
3. Calculate $\boldsymbol{f}_p, \boldsymbol{f}_o, \boldsymbol{f}_f$ from the analytical models by the inputs: œ, $A_{p1}, A_{p2}$, $\boldsymbol{r}_r$, $\dot{\boldsymbol{r}}_r$, $\ddot{\boldsymbol{r}}_r$.

In the step 2, it is necessary to compute the first- and second-time derivatives of $[I \quad \Omega \quad \theta]^T$. They can be computed both numerically and analytically, but this study calculates them from the analytical model of the $J_2$-perturbed osculating orbital elements which is given in Appendix A in [6].

Table 2: Major numerical conditions.

| Item | Value |
|---|---|
| Initial time | 2023 December 21st, 0:00:00 UT |
| Chief initial orbital elements | $a_0 = 6978$ km, $\boldsymbol{e}_0 = [0 \quad 0.0011]^T$, $I_0 = 98°$, $\Omega_0 = 90°$, $\theta_0 = 0°$ |
| Area-to-mass ratio | $(S/m)_1 = 3.6 \times 10^{-3}$ m$^2$kg$^{-1}$ for SC1, $(S/m)_2 = 1.1(S/m)_1$, $(S/m)_3 = 0.9(S/m)_1$ |
| Atmospheric drag | Density: modified Harris-Priester model, $C_d = 2.2$ (drag coefficient) |
| Solar radiation pressure | $P_s = 4.56 \times 10^{-6}$ Pa, $C_s = 0.3$ (specular), $C_a = 0.5$ (absorption) |
| Reference formation | $\alpha$ =20h00m00s, $\delta = 40°$, $\rho_y = 0$ m (SC1), 50 m (SC2), $-50$ m (SC3) |
| Gravity model | Earth spherical harmonic gravity (up to 20 degrees), lunisolar gravity |
| Disturbance setting | Case 1: With gravitational perturbations only.<br>Case 2: With gravitational and non-gravitational perturbations. |
| Simulation time | Four revolutions of the chief orbit<br>(the first two revolutions: the feedforward control disabled, then enabled) |

## IV. Closed-loop simulations

This section shows the performance of the feedforward control presented in Section III for a linear astronomical interferometer. For simplicity, the simulation considers the three-dimensional dynamics (attitude dynamics are not considered) and assumes that both navigation and actuation are perfect.

Table 2 summarizes the numerical conditions. The chief orbit was selected as a sun-synchronous orbit at an altitude of 600 km. The mean eccentricity vector for the chief was selected at the equilibrium for Earth $J_2$ and $J_3$ long-period perturbations. For the area-to-mass ratio was assumed to have an 10% error between spacecraft 1 (SC1) and SC2/SC3. The simple atmospheric model (modified Harris-Priester model [7]) was used for the air drag, and solar radiation pressure (flat plate model) was assumed to be constant. The target observing star was selected to understand the representative control performance; no scientific objectives are intended for this selection. The Earth spherical harmonic gravity up to 20 degrees was considered in addition to lunisolar gravity.

The two scenarios were tested in the simulation. The first one (case 1) in Table 2 was set to understand the pure compensation performance of the major gravitational perturbations under the gravitational effects. The second one (case 2) was set to understand the more realistic performance when the non-gravitational perturbations were applied to orbital dynamics. During the total simulation time of four revolutions of the chief orbit, the feedforward control was disabled for the first two revolutions of the chief orbit (method in Fig. 2), then enabled for the latter two revolutions (method in Fig. 3). For the further numerical setting, the initial position error in the order of $10^{-1}$ m was imposed to each spacecraft. The control frequency was set at 5 Hz. The linear quadratic regulator (LQR) was adopted as the feedback controller, whose feedback gain was selected to minimize the objective function:

$$J = \int_0^\infty (\boldsymbol{x}^T Q \boldsymbol{x} + \boldsymbol{u}^T R \boldsymbol{u})\, dt \tag{14}$$

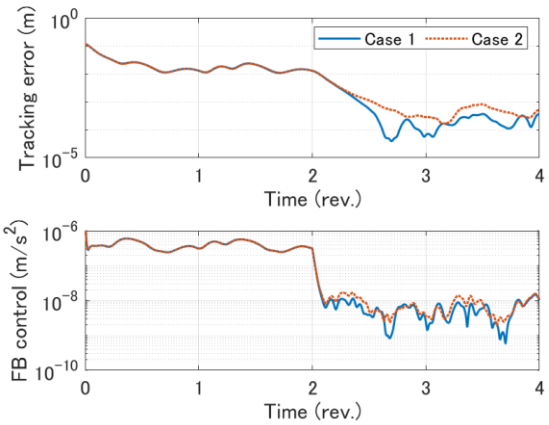


Fig. 6: Tracking error (top) and feedback control acceleration (bottom) for SC2.

where $Q$ and $R$ are the weighting matrix. The diagonal elements of $Q$ and $R$ were non-zero values, and the others were zero. The optimal feedback gain was

$$K = \begin{bmatrix} 14 & -2.4 & 0 & 1.1\times10^4 & 46 & 0 \\ 2.5 & 9.7 & 0 & 46 & 1.0\times10^4 & 0 \\ 0 & 0 & 8.9 & 0 & 0 & 1.1\times10^4 \end{bmatrix} \times 10^{-6} \tag{15}$$

Figure 6 shows the time histories of the tracking errors (norm) and feedback control accelerations (norm). Figures 7 and 8 shows the time histories of the control accelerations for each case. Note that the results on SC2 were presented only, because SC2 and SC3 were placed asymmetrically so that their characteristics were basically the same. As seen in Fig. 6, the position tracking error under disabled feedforward control was maintained in the order of $10^{-2}$ m for both cases, and the feedback controller output the control accelerations in the order of $10^{-7}$ m/s$^2$. After the feedforward control was activated (after the two revolutions), the tracking error further reduced to the order of $10^{-4}$ m, and the feedback control commands also reduced to the order of $10^{-9}$ m/s$^2$ in most durations for each case. Instead, the feedforward

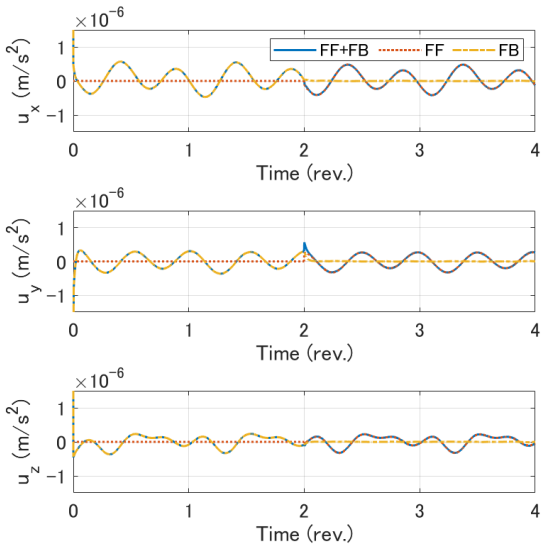


Fig. 7: Control acceleration in the LVLH frame applied to SC2 (Case 1).

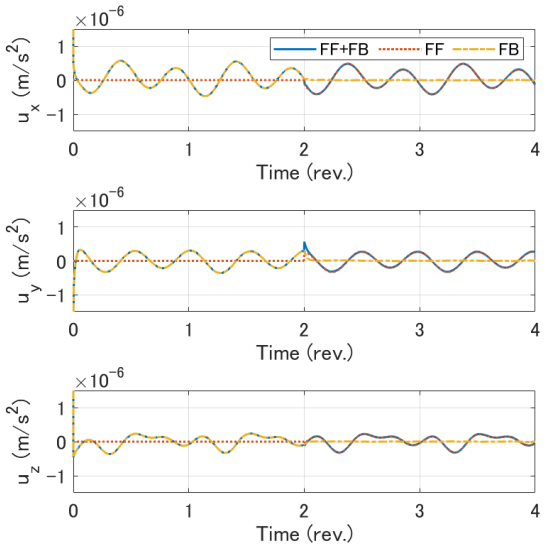


Fig. 8: Control acceleration in the LVLH frame applied to SC2 (Case 2).

control compensated the gravitational perturbations accurately, accounting for the order of $10^{-7}$ m/s$^2$. In Fig. 6, the position control error with feedforward controller for case 2 was larger than that for case 1, but both were maintained with less than $10^{-3}$ m. As seen in these cases, the feedforward compensation of the gravitational perturbations in LEO could reduce the control deviation significantly, by two orders of magnitude even if there exist non-gravitational perturbations.

## V. Conclusions

This study demonstrated the advantage of the feedforward controller to compensate the gravitational perturbations continuously, showing the reduced control deviation by two orders of magnitudes. This technique potentially makes precise formation flying in low Earth orbit much easier. In future work, the performance will be compared when a real-time disturbance estimation is adopted. In addition, the more realistic noise models on sensors/actuators, as well as the modelling errors on atmospheric density and solar radiation pressure, will be adopted to investigate how much robustness the proposed methods have against the systematic and environmental uncertainties.

## Acknowledgments

This study was supported by JSPS KAKENHI Grant Number JP23K13501.

## References

[1] L. F. Penin, Y. Scoarnec, J. M. Fernandez-Ibarz, et al., “Proba-3: ESA’s small satellites precise formation flying mission to study the Sun’s inner corona as never before,” *34th Annual Small Satellite Conference*, Logan, Utah, 2020.

[2] J. T. Hansen and M. J. Ireland, “A linear formation-flying astronomical interferometer in low Earth orbit,” *Publications of the Astronomical Society of Australia*, vol. 37, 2020.

[3] T. Matsuo, S. Ikari, H. Kondo, et al., “High spatial resolution spectral imaging method for space interferometers and its application to formation flying small satellites,” *Journal of Astronomical Telescopes, Instruments, and Systems*, vol. 8, no. 1, 2022.

[4] W. H. Clohessy and R. S. Wiltshire, “Terminal Guidance System for Satellite Rendezvous,” *Journal of the Aerospace Sciences*, vol. 27, no. 9, pp. 653-658, 1960.

[5] D. Izzo, M. Sabatini, and C. Valente, “A New Linear Model Describing Formation Flying Dynamics under J2 Effects”, *Proceedings of the 17th AIDAA National Congress*, vol. 1, pp. 493-500, 2003.

[6] T. Ito, “Formation-flying interferometry in geocentric orbits,” *Astronomy & Astrophysics*, vol. 682, A38, 2024.

[7] I. Harris and W. Priester, “Time-Dependent Structure of the Upper Atmosphere,” *Journal of the Atmospheric Sciences*, vol. 19, no. 4, pp.286-301, 1962.